RSC Applied Polymers

PAPER

View Article Online
View Journal | View Issue

Cite this: *RSC Appl. Polym.*, 2026, **4**, 674

Study of uniaxially stretched single-layer and multi-layer blown films based on poly(butylene adipate-*co*-terephthalate) and inorganic fillers for food and agriculture applications

Debarshi Nath,[a,b] Matias Menossi,[a,b] Ehsan Pesaranhajiabbas,[a,b] Michael R. Snowdon,[b,c] Amar K. Mohanty *[a,b] and Manjusri Misra *[a,b]

Received 1st October 2025,
Accepted 18th December 2025

DOI: 10.1039/d5lp00306g

rsc.li/rscapplpolym

This study develops a biodegradable flexible packaging material using poly(butylene adipate-*co*-terephthalate) (PBAT) with talc or $CaCO_3$ (at 25 wt%) using the blown film extrusion method for flexible packaging applications. The films were produced in single-layer (SL) and tri-layer (TL) configurations. The maximum stretch ratio (SR) obtained for the TL-PBAT/talc25%, TL-PBAT/$CaCO_3$25%, and SL-PBAT/$CaCO_3$25% were 4, 5.5, and 6, respectively. The mechanical properties of the PBAT/talc films were better than the PBAT/$CaCO_3$ films for both stretched and unstretched films. With uniaxial orientation in the machine direction, the tensile strength, impact strength, and modulus increased for all films while the elongation at break decreased. The maximum improvement was shown for tensile strength, where this property increased by 250%, 400%, and 300% for TL-PBAT/talc25%, SL-PBAT/$CaCO_3$25%, and TL-PBAT/$CaCO_3$25%, respectively, after stretching to the maximum SR. This is attributed to strain-induced crystallization and strong alignment of polymer chains in the machine direction. This is evident from the improvement of barrier performance of the films upon stretching, also attributed to the increase in crystallinity of the films. The measurement of percentage crystallinity was conducted using DSC and XRD techniques, where the crystallinity of the samples increased with an increase in SR. Although other factors also influence the improvement of stretched film performance, an increase in crystallinity is considered one of the most important factors. Morphological analysis of the samples shows better talc dispersion than $CaCO_3$ and a strong orientation of the matrix in the stretching direction.

1. Introduction

Current evidence has shown that plastic waste has severe consequences for our planet. To put matters into perspective, global plastic consumption is expected to triple from 460 million tonnes (Mt) in 2019 to 1321 Mt by 2060, driven primarily by economic growth.[1] Total plastic waste is set to increase from 353 Mt to 1014 Mt during the same period, with the main contributors being packaging materials.[1] The packaging industry has grown to be one of the biggest industries in the world, as commercializing products without effective packaging solutions would not be feasible. Flexible plastic packaging has become a major waste format that poses a challenge to the recycling stream, a large segment of which comprises single-use plastic packaging that is primarily accumulated in landfills due to widespread and indiscriminate use.[2] Of all packaging materials, flexible plastic packaging accounts for the largest percentage of packaging units (36%).[3] Despite international efforts and global initiatives to recycle plastic packaging waste, ~79% of all plastic waste ends up in landfills and the natural environment, while only 9% is recycled, with the remaining 12% incinerated.[4] Transitioning from a fossil fuel-dependent economy to a sustainable economy requires materials with performance comparable to those of existing petrol-based materials but exhibiting low or net-zero carbon emissions.[4,5] Therefore, to address this issue, biodegradable polymers with better end-of-life options have gained popularity in research and industry alike. In particular, polymers capable of biodegradation under home-composting conditions are desirable as a packaging material.[6]

[a]*Department of Interdisciplinary Engineering, College of Engineering, Thornbrough Building, University of Guelph, 50 Stone Road East, Guelph, Ontario, Canada. E-mail: mohanty@uoguelph.ca, mmisra@uoguelph.ca*
[b]*Bioproducts Discovery and Development Centre, Department of Plant Agriculture, Crop Science Building, University of Guelph, 50 Stone Road East, Guelph, Ontario, Canada*
[c]*Sustainable Packaging Team, Automotive and Surface Transportation, National Research Council Canada, Advanced Manufacturing Research Facility, 2690 Red Fife Road, Centreport, Manitoba, Canada, R4B 0A6*

Poly(butylene adipate-*co*-terephthalate) (PBAT), an aliphatic–aromatic copolyester, is an amorphous polymer exhibiting high ductility with home-composting capabilities at a particular thickness. PBAT is particularly popular for making flexible packaging materials due to its excellent film-blowing capabilities, with high impact strength and toughness, and low price compared to other bioplastics.[7] PBAT is synthesized *via* condensation polymerization of terephthalic acid, adipic acid, and 1,4-butanediol. Even though PBAT is biodegradable, it suffers from disadvantages such as poor modulus, heat resistance, and gas barrier performance.[8] Extensive research has focused on enhancing PBAT's properties and processing, including the addition of fillers such as talc,[8] kaolin,[9] calcium carbonate ($CaCO_3$),[10] and wollastonite.[7] Filler addition helps in enhancing the elastic modulus, barrier performance, and ease of processing PBAT, and also lowers its cost of production. Talc and $CaCO_3$ are reinforcing fillers, commonly used, to enhance PBAT properties as filler incorporation is amongst the most economical methods to modify the mechanical and crystalline characteristics of bioplastic while preserving its biodegradation properties.[8,11]

Multilayer packaging film is an innovative approach that combines the unique properties of various polymers to develop a flexible packaging material with superior performance in moisture and gas barrier resistance, strength, and good sealing capacity compared to monolayer films.[12] Monolayer films typically cannot meet the requirements of high-performance flexible films designed for specific applications. Due to their advantages, multilayer films are increasingly becoming popular in the food and packaging industries.[13] Multilayer flexible films are created using coextrusion and lamination techniques to achieve the specific properties required for different uses.[3] Through coextrusion, films can be developed with distinct polymer layers, each engineered to provide particular properties such as sealing ability, high strength, low permeability, and resistance to impact, along with reducing film thickness while improving or maintaining flexible-film attributes.[3] Scaffaro *et al.*[14] developed polylactic acid/carvacrol and Bio-flex®/nanoclay bilayer films using the coextrusion technique for food packaging applications. The volatile carvacrol (used as an antimicrobial agent) is protected by the presence of a Bio-flex®/nanoclay layer, and the film shows the individual properties of both layers. Palmieri *et al.*[15] explored the benefits of a tri-layer bioplastic film with a nanoclay-filled layer as its core layer to utilize the specific advantages of each layer. However, multilayer films are very difficult to recycle as they contain different types of polymers. As a result, to facilitate recycling and targeting specific functionalities, Wei *et al.*[16] developed mono-material polyethylene (PE)-based films that exhibited a good mechanical–barrier performance balance required for packaging applications. Guleria *et al.*[17] also developed PE films that can be used as an outer layer for mono-material PE-based multilayer packaging. The film was mechanically stretched in the machine direction to enhance outer layer performance.

Multilayer films offer a versatile approach to tailoring film properties; however, another important technique that enhances the polymer properties by modifying their microstructures is uniaxial orientation, using the machine direction orientation (MDO) technique. It is a commercially relevant technique that draws the polymeric film in the machine direction using the force generated by two rollers rotating in opposite directions at different speeds at a particular ratio.[18,19] This stretching process takes place at a temperature above the glass transition temperature (T_g) but below the temperature at which the polymer melts. Nie *et al.*[20] analyzed the microscopic images of stretched polypropylene films and reported the transformation of initial spherulitic structures to a fibrillar structure having thick fibrils in the machine direction. They reported that this change in morpholog contributed to the modification of film performance. Itabana *et al.*[8] in their study developed uniaxially stretched PBAT/talc films. They reported that film stretching improved the modulus and barrier performance due to an increased crystallinity percentage in the films caused by the MDO process. A comparable pattern was also noted by Nath *et al.*[19] for BioPBSA and talc-filled composites.

The goal of this study was to produce uniaxially stretched PBAT-based tri-layer mono-material films filled with talc or $CaCO_3$ using coextrusion technology. The study was conducted to compare both single-layer (SL) and mono-material tri-layer (TL) films and study the impact of film type on material properties. This allows for a better comprehension of how the multilayer structure itself impacts performance, independent of material composition. Furthermore, the TL and SL films were uniaxially stretched to understand the effect of the MDO process on the films. To assess the properties, the mechanical, thermal, barrier, and morphological characteristics of the films were studied under both unstretched and different stretch ratio (SR) conditions. Despite the MDO process being used industrially for many decades, based on the literature review, there have been very few studies on MDO's impact on mineral-filled multilayer films. Therefore, this research tries to fabricate uniaxially stretched high-performance TL and SL composite films for use in the agriculture, food, and other packaging industries.

2. Experimental section

2.1. Materials

The PBAT polymer (grade TH801T) was sourced from Xinjiang Blue-Ridge Tunhe Polyester Co. (China). As specified in the technical datasheet (TDS), this aliphatic–aromatic copolyester has a density of 1.21 g cm^{-3} and a melt flow index (MFI) ranging from 3.5 to 4.5 g per 10 min (measured at 190 °C with a 2.16 kg load). Talc (Jetfine 3CC, CAS No. 14807-96-6) was supplied by Imerys, USA, while calcium carbonate ($CaCO_3$) powder (CAS No. 471-34-1) was obtained from Guangdong QiangDA New Materials Technology Co. Ltd, China, with specific gravities of 2.8 and 2.7 and median diameter particle sizes of 0.9 μm and 2.5 μm, respectively, according to their TDS.

2.2. PBAT/inorganic filler composites *via* melt extrusion

Composite pellet comprising of PBAT with 25 wt% talc or $CaCO_3$ as fillers were produced using a Micro-27 co-rotating twin-screw extruder (Leistritz Advanced Technologies Corporation, USA). The filler content of 25 wt% was selected based on prior optimization from previous studies showing the best balance between cost, performance and processability.[7,19] To ensure consistency, each formulation was precisely weighed and thoroughly mixed in zip-lock bags before being fed into the extruder hopper at a feed rate of 8 kg h^{-1}. The extrusion process was carried out with a uniform temperature of 160 °C across all 12 zones, with the screw speed set at 100 rpm. The extruded polymer melt was then cooled in a water bath, air-dried, and processed into pellets. After measuring the moisture level, the pellets were subsequently dried overnight at 65 °C before being sealed in aluminum bags for storage.

2.3. Blown film from PBAT/inorganic filler

PBAT composite films containing 25 wt% filler were produced using a Collins Blown Extrusion Machine (Collins Lab & Pilot Solutions, Inc., USA). The extrusion process was conducted with the lab line single-screw extruder with a set temperature profile of 30 °C, 155 °C, 160 °C, 160 °C, and 165 °C across five zones while maintaining a screw speed of 50 rpm. The RWT 40-5 type blown film die temperature was held constant at 160 °C. As the molten polymer came out of the die, the polymer formed a bubble using the film blowing unit type BL 180/600 with dual lip air ring, which was expanded by 33% and drawn by take-up rollers operating at 1.5 m min^{-1}, resulting in a continuous thin film wound onto a winder. To ensure uniformity, nip rollers flattened the bubble before collecting. The single-layer films were prepared using one extruder, while tri-layer films were produced by using three separate extruders under conditions mentioned above. The tri-layer films were developed in AAA configuration (where A refers to the same material for each extruder). During extrusion, the film was oriented in the machine direction (MD) by the nip rollers, while bubble inflation-induced orientation was in the transverse direction (TD). Table 1 details the developed formulations and their corresponding SR values.

For stretching, the developed films were fed to the MD orientation unit, where the films were stretched at a particular SR at 40 °C. All the stretched samples were characterized for their properties except for the neat tri-layer PBAT films, as the films cannot be separated/opened after stretching.

The method described by Pietrosanto *et al.*[21] was employed to determine the blow-up ratio (BUR). This involved first calculating the bubble diameter by multiplying the film's lay-flat width by a factor of 0.637. The resulting value was then divided by the die diameter, as illustrated in eqn (1):

$$\text{Blow-up ratio (BUR)} = \frac{0.637 \times \text{lay-flat width}}{\text{die diameter}} \quad (1)$$

The draw-down ratio (DDR) is a key parameter in the film blowing process. Here, the MDO was controlled by adjusting the haul-off speed as the polymer emerged from the die. The relationship between DDR and BUR is defined by eqn (2), following the approach presented by Mallegni *et al.*:[22]

$$\text{Draw down ratio (DDR)} = \frac{\text{width of die gap}}{\text{film thickness} \times \text{BUR}} \quad (2)$$

The width of the die gap was configured to 0.80 mm.

3. Characterization of PBAT/inorganic filler composites

3.1. Mechanical properties

The mechanical performance of the films was assessed using a universal testing machine (Instron 3382, USA) in accordance with ASTM D882 guidelines. Film thickness was determined with a dial thickness gauge (Japan) with a precision of 0.01 mm, based on the average of three measurements per sample. For films with an elongation at break exceeding 100%, the grip separation was set to 50 mm, and the crosshead speed to 500 mm min^{-1}. When elongation at break ranged between 20% and 100%, these parameters were adjusted to 100 mm and 50 mm min^{-1}, respectively, following ASTM D882 recommendations. Each formulation was tested using ten specimens, with results

Table 1 Composition of PBAT composite film formulations made in this study at various SR values, along with the blow-up ratio (BUR) and draw-down ratio (DDR) for each formulation

Formulation	Stretch ratio	Identification	PBAT (wt%)	Inorganic filler (wt%)	BUR	DDR
Tri-layer neat PBAT	Unstretched (UNST)	TL-PBAT UNST	100	0	4.75	4.94
Tri-layer PBAT/talc25%	Unstretched (UNST)	TL-PBAT/talc25% UNST	75	25	4.83	2.54
	2	TL-PBAT/talc25% SR2				
	4	TL-PBAT/talc25% SR4				
Single-layer PBAT/$CaCO_3$25%	Unstretched (UNST)	SL-PBAT/$CaCO_3$25% UNST	75	25	2.44	4.55
	2	SL-PBAT/$CaCO_3$25% SR2				
	4	SL-PBAT/$CaCO_3$25% SR4				
	6	SL-PBAT/$CaCO_3$25% SR6				
Tri-layer PBAT/$CaCO_3$25%	Unstretched (UNST)	TL-PBAT/$CaCO_3$25% UNST	75	25	4.88	2.64
	2	TL-PBAT/$CaCO_3$25% SR2				
	4	TL-PBAT/$CaCO_3$25% SR4				
	5.5	TL-PBAT/$CaCO_3$25% SR5.5				

expressed as the mean ± standard deviation (SD). The films were tested in both the MD and transverse direction (TD).

The impact strength of the unstretched and stretched films was assessed using the dart drop impact strength as per ASTM D1709 (method A) to determine the weight at which impact failure occurs, expressed in grams (g). The weight of the dart was 33 g. A Qualitest dart drop impact tester (Model DX-8165AB) was used to do this experiment. As per the standard, each sample was tested at least 20 times to determine the impact failure weight.

3.2. Morphology

To analyze the morphology of the blown film samples, they were examined using scanning electron microscopy (SEM), specifically with a Phenom Pro X (Netherlands), operating at a voltage of 10 kV. To prepare the samples for SEM imaging, liquid nitrogen (N_2) was used to cryo-fracture them by immersing the samples, which allowed for the examination of the cross-sectional structure. Film samples oriented in the MD were mounted onto an aluminum stub with double-sided carbon tape and coated with gold using a sputter coater (Cressington Sputter Coater 108) to minimize electrical charging during imaging.

3.3. Differential scanning calorimetry (DSC)

Differential scanning calorimetry (DSC) measurements were performed using a Q200 calorimeter (TA Instruments, USA) with an N_2 flow rate of 50 mL min^{-1} and a heat–cool–heat cycle. Sample weights ranged from 5 to 12 mg, and samples were placed in aluminum pans for testing. The process began by heating the samples from −70 °C to 200 °C at a rate of 10 °C min^{-1}, followed by a 2-minute isothermal hold to erase any thermal history of the polymers. Afterward, the samples were cooled from 200 °C to −70 °C at the same rate, with another 2-minute equilibration period. The final stage involved reheating from −70 °C to 200 °C at 10 °C min^{-1}. Key thermal properties, including melting temperature (T_{melt}), crystallization temperature (T_{cryst}), T_g, and the enthalpy of melting (ΔH_{melt}) were obtained from the cooling and heating cycles. The crystallinity degree ($X_{C,DSC}$) of PBAT in the polymer blends was calculated using eqn (3):

$$X_{C,DSC}(\%) = \frac{\Delta H_{melt}}{\Delta H^{\circ}_{melt} \times X_f} \quad (3)$$

ΔH_{melt} represents the enthalpy of melting, while ΔH°_{melt} refers to the theoretical enthalpy for 100% crystalline PBAT, which is documented as 114 J g^{-1}.[23] The melting enthalpy ΔH°_{melt} was determined by integrating the area under the melting peak, from its onset to the end, using TA Universal Analysis software.

X_f denotes the weight fraction of PBAT in the sample. The test was conducted in duplicate, and the results are presented as the average ± SD.

3.4. X-Ray diffraction spectroscopy

Powder X-ray diffraction was used to measure the percentage crystallinity of the samples, using CuKα (λ = 1.5418 Å) radiation generated at a voltage of 45 kV and a current of 40 mA. Measurements were conducted using a PANalytical Empyrean diffractometer. The instrument was set up in a reflection geometry and utilized a nickel-filtered copper K-alpha (CuKα) radiation source along with a PIXcel1D linear detector.

The data were collected in the 5 to 60° 2θ range for the film sample in a stationary, flat sample holder. The data were collected and then processed using the Data Collector and HighScore Plus (version 4.1) software, respectively. The percentage crystallinity of both unoriented and uniaxially stretched film samples was calculated using eqn (4), by comparing the area under the crystalline section (A_C) of the spectrum to the total area (A_T) under the diffractogram.[24,25] For neat PBAT film, the broad halo with minor peaks was considered as the crystalline region for calculation purposes. Origin Pro 20 software was utilized for these crystallinity calculations:

$$X_{C,XRD}\ (\%) = \frac{A_C}{A_T} \times 100. \quad (4)$$

3.5. Dynamic mechanical analysis

Dynamic Mechanical Analysis (DMA) of the film samples was conducted to determine the storage modulus and damping factor (tan δ) of the film samples. A Q800 DMA instrument (TA Instruments, USA) was used to perform the test in the temperature range of −50 to 40 °C at a heating rate of 2 °C min^{-1} in multifrequency-strain mode. The samples were subjected to sinusoidal deformation at 0.1 Hz frequency and 20 μm amplitude.

3.6. Barrier properties

The barrier properties of PBAT/inorganic filler composites were evaluated for oxygen permeability using a coulometric sensor (ASTM D3985). The tests were conducted at 0% relative humidity and 23 °C with a sample area of 5 cm^2, using a Mocon OX-TRAN model 2/21 (USA) machine. During the process, oxygen gas permeating through the specimens was captured by N_2 and detected by the sensor. The oxygen permeability (OP) was then quantified based on the measured amount of oxygen gas. For water vapor permeability (WVP) assessment, the samples were tested with a Permatran-W 3/33 instrument (Mocon, USA), following ASTM F1249 standards. Each sample, sized at 5 cm^2, was positioned within the module's dual-chamber system under conditions of 37.8 °C and 100% relative humidity. High-purity N_2 was used as the carrier gas, flowing at a rate of 100 cm^3 min^{-1}. A 30-minute purge phase was conducted to eliminate any residual moisture before testing. Sections from the developed film were placed between aluminum frames for each analysis.

3.7. Contact angle and surface energy

The contact angles of water (polar liquid) and diiodomethane (non-polar liquid) on the PBAT/inorganic filler composite blown films were measured using a Ramé-Hart Standard Goniometer equipped with a high-speed digital camera (260-U1, USA) at room temperature. The samples were cut into

2×2 cm^2 pieces and put on the platform attached to the instrument. A 5 μL droplet of water or diiodomethane was dispensed onto the surface of each specimen using a glass syringe connected to the contact angle goniometer. After approximately 5 seconds, the contact angles on both sides of the droplet were measured with DROPimage Advanced software. The measurements were performed with a resolution of ±0.01°, an accuracy of ±0.1°, and a stage angle set at 0°. The experiment was done in triplicate on different regions of the sample, with the results presented as average ± SD. The harmonic and geometric mean surface tensions of the PBAT/inorganic filler composite blown films were also determined using DROPimage Advanced software, which utilized the measured contact angles of the two liquids along with their known surface tension values to determine the polar, dispersive, and total surface components.

4. Results and discussion

4.1. Mechanical properties

There are various approaches to modifying the mechanical performance of flexible films made from biodegradable polymers. One common approach is to integrate inorganic fillers into the biopolymer matrix, which can contribute to improvement in mechanical properties, specifically the stiffness of the material. The efficiency level of these fillers to enhance the mechanical performance of these polymers is highly dependent on several factors, including their particle shape, their dispersion and distribution through the polymer matrix during the processing, and their interaction with the polymer matrix. Another approach is to stretch polymer film, either uniaxially or biaxially, to align its macromolecules in a specific direction. In this study, both approaches were utilized and investigated for tuning the mechanical performance of PBAT films.

Table 2 presents the tensile modulus, tensile strength, and elongation at break of different PBAT films in the MD. The transverse direction (TD) data and stress–strain curves of the samples are provided as supplementary information. The data for unstretched and stretched monolayer neat PBAT and PBAT/talc biocomposite films were obtained from previous work done in our laboratory.[8] The reinforcing effect of both talc and $CaCO_3$ can be noticed in both monolayer and tri-layer PBAT films. For monolayer films, the incorporation of 25 wt% talc and calcium carbonate resulted in 159% and 127% improvement in tensile modulus in the MD, respectively. Similarly, an enhancement in the MD modulus of tri-layer PBAT composite films could be observed after incorporating these fillers. However, along with this improvement in stiffness, both tensile strength and elongation at break of the PBAT biocomposite films decreased in both single and tri-layer films. The decrease in tensile strength and deformability of films by incorporation of fillers is a well-known phenomenon for most polymers, which is mainly explained by the fact that filler particles act as stress concentration within the polymer matrix, facilitating crack formation in and fracture of the material.[26,27] Comparing the reinforcing effect of two types of fillers, it is evident that talc provides more effective reinforcement. This difference mainly lies in the difference between the shapes of particles comprising these fillers. Talc usually has particles in platelet shapes with higher aspect ratios, while calcium carbonate has particles with low aspect ratios. Talc has aspect ratios in the range 5–20 in powder form.[28] Generally, the particles with a higher aspect ratio can contribute to higher stiffness when added to a polymer matrix.[29] Moreover, in the case of PBAT/talc films, no notable difference can be noticed in the mechanical properties of monolayer and tri-layer films.

Table 2 also compares the effect of uniaxial stretching (in the MD) on the mechanical behavior of films. In our previous study[8] on monolayer films made from PBAT and 25 wt% talc, we observed that stretching in the MD can significantly improve both tensile strength and modulus in this direction. A similar trend was also observed in the current study for tri-layer PBAT/talc films as well as PBAT/calcium carbonate films (both SL and TL). For the TL-PBAT/talc25% UNST film, tensile strength and modulus moderately improved from 20 MPa and 137 MPa to 39 MPa and 163 MPa, respectively, after stretching the TL films to SR 2. When the SR was increased to 4 (SR = 4), a significant boost was achieved in these properties (tensile strength and modulus reached 70 MPa and 417 MPa, respectively), accompanied by a reduction in elongation at break, which was reduced to 74% (from 457%). Similarly, stretching of both SL-PBAT/$CaCO_3$25% and TL-PBAT/$CaCO_3$25% films helped improve the tensile strength and modulus of the film at the expense of a reduction in film deformability, which is proportional to the SR.

For the unstretched SL-PBAT/$CaCO_3$25% and TL-PBAT/$CaCO_3$25% films, the tensile strengths were 18 MPa and 12 MPa, and the corresponding tensile moduli were 84 MPa and 76 MPa, respectively. After stretching to the maximum SR, the tensile strength and modulus increased to 90 MPa and 48 MPa for the SL-PBAT/$CaCO_3$25% film, and to 584 MPa and 289 MPa for the TL-PBAT/$CaCO_3$25% film. This corresponds to an improvement of approximately 400% (tensile strength) and 595% (modulus) for the single-layer film, and 300% (tensile strength) and 280% (modulus) for the tri-layer film relative to their unstretched condition.

On the other hand, in the TD (Table S1), a reverse trend could be observed: tensile strength decreased in the TD after stretching, while there was a slight improvement in elongation at break of films by increasing the SR in both types of biocomposites. The enhancement of tensile strength and modulus in the MD after stretching can be explained by the alignment of the polymer macromolecules in the MD as well as enhanced crystallinity (as observed in both the DSC and XRD analyses) in the material, which increases the resistance of the film against deformation.[30] As a result of the MDO, highly oriented macromolecules in the MD have less mobility, which correlates with the lower elongation at break of stretched films in the MD. Additionally, the reduced elongation in the MD was attributed to the alignment and confinement of polymer chains

Table 2 Mechanical properties of all the SL and TL films in the machine direction

Formulation	Stretching ratio	Film thickness (mm)	Tensile strength (MPa)	Tensile modulus (MPa)	Elongation at break (%)	Dart drop impact (g)
SL-PBAT[a]	Unstretched	0.034	35 (±4.8)	37 (±13.6)	520 (±53.1)	29.5
TL-PBAT	Unstretched	0.034	30 (±5.1)	62 (±9.5)	618 (±48.2)	22
SL-PBAT/talc25%[a]	Unstretched	0.049	18 (±5.1)	96 (±28.8)	477 (±13.7)	13.5
	2	0.031	39 (±5.7)	102 (±11.6)	233 (±12.9)	Not tested
	4	0.017	69 (±6.6)	449 (±41.2)	77 (±6.5)	22
TL-PBAT/talc25%	Unstretched	0.038	20 (±1.1)	137 (±25.0)	457 (±22.4)	24.5
	2	0.05	39 (±2.5)	163 (±10.7)	281 (±15.1)	46
	4	0.023	70 (±4.9)	417 (±25.6)	74 (±10.0)	51.5
SL-PBAT/ $CaCO_3$25%	Unstretched	0.072	18 (±1.5)	84 (±7.1)	548 (±36.3)	32.5
	2	0.055	33 (±4.6)	72 (±10.2)	288 (±20.0)	29.5
	4	0.027	68 (±6.5)	232 (±30.5)	142 (±14.9)	34
	6	0.021	90 (±7.4)	584 (±45.5)	40 (±7.5)	37.5
TL-PBAT/ $CaCO_3$25%	Unstretched	0.062	12 (±1.4)	76 (±8.5)	402 (±25.6)	62.5
	2	0.049	32 (±3.8)	70 (±6.6)	296 (±13.0)	49.5
	4	0.031	46 (±7.0)	186 (±28.6)	96 (±8.1)	80
	5.5	0.021	48 (±5.5)	289 (±32.2)	55 (±7.1)	79

[a] Data taken from Itabana *et al.*[8]

during stretching, which restricted the movement of the amorphous regions.[19,30] The remarkable enhancement in the mechanical performance of the most highly stretched films could be linked to fibrillation, as it is well established in the literature that when polymer lamellae are subjected to uniaxial orientation, they begin to transform into fibrillar structures.[19,31]

Interestingly, when comparing the stretched SL and TL films at similar SR values, the SL films consistently exhibited better mechanical properties than the TL films (Table 2). This trend was observed for both talc- and $CaCO_3$-based films. One possible reason could be the initiation of delamination between different layers during the uniaxial orientation process. These defects might negatively impact the mechanical properties. Also, each layer might stretch unevenly, resulting in different modulus, strength, or crystallinity values for each layer.

The dart drop impact measurements were conducted to assess the impact strength of the films (Table 2). The impact strength of a material is dependent on several factors, including film thickness, load application rate, method of filler mixing, inherent properties of the polymer matrix, such as packing, chain length, and interfacial interaction between polymer and filler. The impact strength of SL-PBAT film was 29.5 g [value taken from ref. 8] while that of TL-PBAT was 22 g. For the unstretched SL film, the addition of $CaCO_3$ had a minimal effect on impact strength, increasing it from 29.5 (neat SL PBAT) to 32.5 g. In contrast, the unstretched tri-layer film showed a substantial enhancement upon adding $CaCO_3$. The impact strength increased from 22 g (neat TL PBAT) to 62.5 g for the TL-PBAT/$CaCO_3$ film. However, for talc-filled unstretched SL and TL films, the impact strength was reduced compared to neat SL-PBAT films. This could be due to the higher ductility of $CaCO_3$-loaded films compared to the talc ones, which resulted in higher tolerance towards failure. After uniaxial stretching of all TL and SL films, the impact strength increased considerably. The maximum values reached were 51.5 g for TL-talc (at SR 4), 80 g for TL-$CaCO_3$ (at SR 4), and 37.5 g for SL-$CaCO_3$ (at SR 6), corresponding to increases of 51%, 15%, and 28% compared to their unstretched counterparts.

It has been reported in the literature that the tensile and impact strength of MD-oriented films enable superior properties.[32] This is attributed to the increased orientation of the polymer chains. The dart drop resistance property, which is very much dependent on the thickness of the films, showed an increment in the value for the stretched film (at the highest SR) even though the thickness reduced after film stretching. Godshall *et al.*[33] also reported that dart drop impact strength shows an increment as the film gauge is decreased for HDPE films. This can be attributed to the increased stiffness of the films after stretching (due to polymer chain orientation), which enables them to absorb more impact energy, thereby compensating for the reduction in thickness.[34]

4.2. Morphology

The morphology of the developed films (in both their stretched and unstretched forms) is illustrated in Fig. 1(a–g). Fig. 1(a) presents the microstructure of the neat tri-layer PBAT film. The micrograph shows a relatively smooth film cross-section without the presence of any voids or gaps. The visible texture on neat TL-PBAT films results from PBAT's high ductility, which causes linear deformation during cryofracture.[8,35] Now coming to the unstretched composite films [Fig. 1(b), (d) and (f)], $CaCO_3$ and talc particles are clearly visible within the film matrix. In the SEM images, the $CaCO_3$ particles appear as white dots with a relatively smoother structure, whereas the talc-based composites exhibit a coarser surface with a platelet-like structure throughout the matrix. However, the individual layers were not observed in the micrographs since the tri-layer is composed of a mono-material, which makes it harder to isolate individual layers. In the SEM images, the $CaCO_3$ filler exhibited a somewhat irregular morphology with uneven

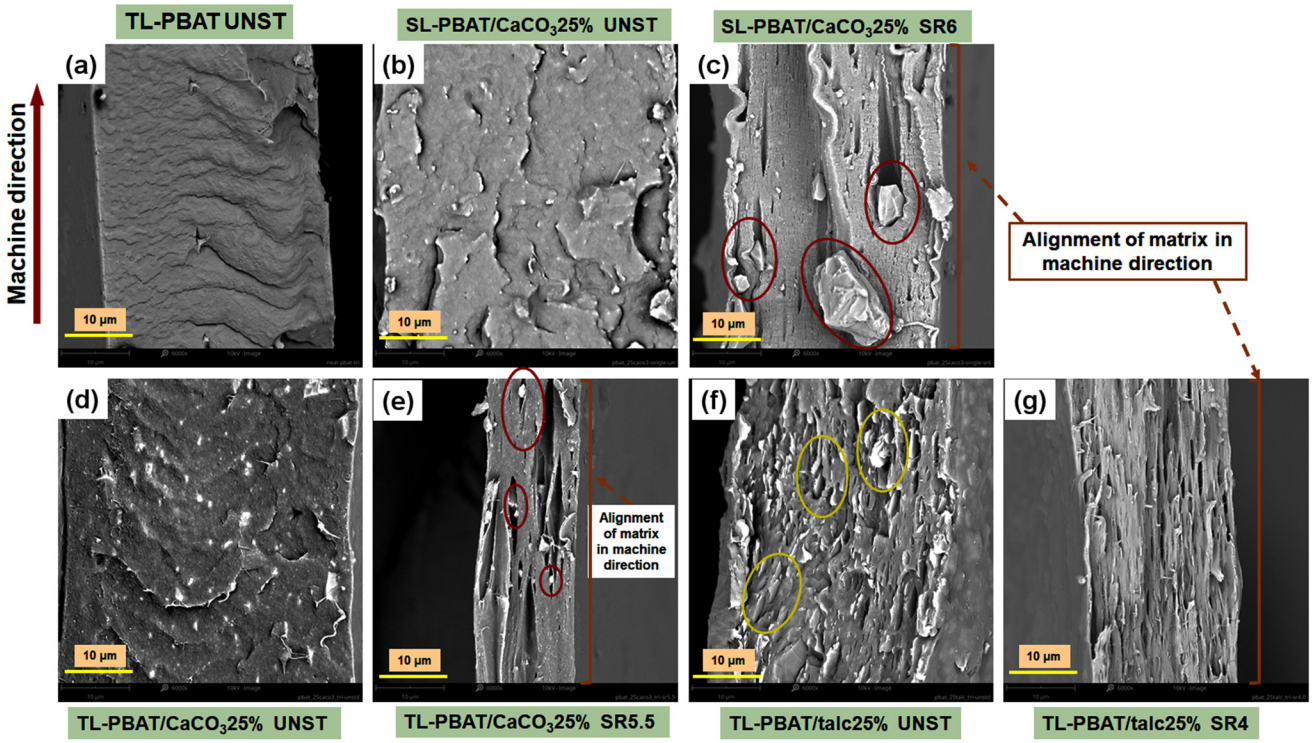

Fig. 1 Morphology of single-layer and tri-layer films: (a) TL-PBAT UNST, (b) SL-PBAT/$CaCO_3$25% UNST, (c) SL-PBAT/$CaCO_3$25% SR6, (d) TL-PBAT/$CaCO_3$25% UNST, (e) TL-PBAT/$CaCO_3$25% SR5.5, (f) TL-PBAT/talc25% UNST, and (g) TL-PBAT/talc25% SR4; the red and yellow circles highlight $CaCO_3$ and talc particles, respectively, in the composite films.

size,[36] whereas the talc particles showed a platelet-like layered structure, which is the reason for the better properties of unstretched talc films. Also, the $CaCO_3$ particles agglomerated to form both large and small clusters within the matrix, which was not visible in talc-based films (which can be better observed in the stretched films).

Upon uniaxial orientation of the SL and TL films, the matrix and fillers exhibited strong orientation towards the MD [Fig. 1(c), (e), and (g)]. The stretched $CaCO_3$ films (both single and tri-layer) exhibited a high concentration of cavities behind the large, irregularly shaped agglomerated $CaCO_3$ particles in the direction of the stretching, which amplified the voids in the matrix (as $CaCO_3$ agglomerates could not be dispersed when stretched). However, the talc-based films showed much better matrix orientation and filler dispersion in the stretched samples with much smaller cavities [Fig. 1(g)]. This coincides with the observation for the highest SR films demonstrating the best overall properties. During MDO processing, the original spherulitic crystal structure of the unstretched film transforms into a fibrillar form that leads to higher percentage crystallinity, consequently affecting the barrier and mechanical properties.[8,31]

4.3. Differential scanning calorimetry

The DSC studies were conducted mainly to estimate the crystalline content and qualitatively analyze the thermal transitions and behavior of the film samples. The first heating and first cooling cycle data of all the samples are provided in Table 3. The DSC curves are presented in the supplementary information. The T_g values of all the film samples were in the range of −27 to −35 °C. There was no significant change in the T_g of either the SL or TL films after uniaxial stretching (based on DSC). Similar observations have been reported in other studies, where the T_g of PBAT-based composite films remained unchanged following uniaxial orientation.[7,8,37]

The T_m of the film samples exhibited a different trend compared to T_g. For the neat TL-PBAT UNST sample, the T_{melt} was 119.4 °C, and it remained largely unchanged with the incorporation of talc and $CaCO_3$. Menossi *et al.*[7] similarly reported that the addition of wollastonite to the PBAT matrix did not cause any significant change in T_{melt}. However, after stretching, the T_{melt} of all TL-PBAT/talc25% and SL-PBAT/$CaCO_3$25% films decreased, likely due to the formation of lower-melting, imperfect crystals.[38] The T_{crys} of neat TL-PBAT UNST films was 75.6 °C, which changed to 71 °C for unstretched SL-PBAT/$CaCO_3$25% and TL-PBAT/$CaCO_3$25%, which could be due to filler agglomeration impeding the crystallization of the PBAT, causing it to occur at a lower temperature during the cooling cycle; but for TL-PBAT/talc25% UNST film, T_{crys} increased to 89.4 °C (Table 3). This is because of better nucleation ability of talc than $CaCO_3$, which can accelerate the crystallization process, resulting in higher T_{crys} during the cooling cycle.[39] However, the uniaxial stretching process did not alter the T_{crys} of the films substantially, and there was no apparent trend in the variation in this property.

Table 3 DSC analysis of neat PBAT and PBAT-composite films

Formulation	Stretch ratio	T_{melt} (°C)	T_{crys} (°C)	$X_{c,DSC}$ (%)
TL-PBAT UNST	Unstretched	119.4 (±1.8)	75.6 (±1.2)	7.4 (±1.9)
TL-PBAT/talc25%	Unstretched	118.0 (±0.4)	89.4 (±0.9)	14.3 (±0.0)
	2	114.4 (±0.1)	89.3 (±0.3)	18.6 (±0.5)
	4	116.0 (±0.6)	89.0 (±1.1)	23.6 (±4.3)
SL-PBAT/$CaCO_3$25%	Unstretched	119.4 (±2.7)	71.0 (±0.1)	16.6 (±0.7)
	2	120.6 (±1.1)	71.1 (±0.2)	17.9 (±0.7)
	4	114.5 (±0.4)	79.8 (±2.1)	18.3 (±0.4)
	6	111.6 (±1.3)	78.9 (±4.5)	23.7 (±1.3)
TL-PBAT/$CaCO_3$25%	Unstretched	116.9 (±3.2)	73.8 (±0.2)	12.1 (±0.1)
	2	116.8 (±1.7)	73.9 (±0.1)	16.5 (±0.5)
	4	115.4 (±0.8)	73.6 (±0.4)	17.3 (±0.2)
	5.5	116.0 (±1.1)	73.3 (±1.2)	15.1 (±0.2)

Table 3 also presents the percentage crystallinity of the film obtained from DSC studies. The $X_{c,DSC}$ of neat TL-PBAT UNST was 7.4%; our previous work also reported that a low $X_{c,DSC}$ for neat SL PBAT (~11%).[8] This value increased almost twofold when talc and $CaCO_3$ were added for both SL and TL films. It has been reported in the literature that inorganic fillers like talc and $CaCO_3$ can serve as nucleating agents, leading to an increase in the $X_{c,DSC}$ of the composite films.[40,41] This improvement in percentage crystallinity might be one of the reasons for the enhancement of the mechanical properties of all the films compared to neat PBAT films.

After the uniaxial process, the $X_{c,DSC}$ of the films increased with an increase in SR. This indicates a strong correlation between the SR and the percentage crystallinity achieved. This phenomenon can be attributed to strain-induced crystallization, which promotes the formation of additional nucleation sites.[42] These findings are further supported by the results from XRD analysis. A similar trend was reported for PBAT and silane-treated wollastonite films, where the $X_{c,DSC}$ increased with an increase in SR.[7] However, for TL-PBAT/$CaCO_3$25%, the highest $X_{c,DSC}$ was observed at SR 4.0, following which it decreased nominally. This suggests that the TL films might have a maximum $X_{c,DSC}$ limit beyond which additional stretching does not enhance crystallinity.

Although this increase in crystallinity in the composite film might influence the biodegradation behavior of the films, in most cases, degradation starts from the amorphous phase, and the material crystallinity increases as the biodegradation process continues.[2] Also, higher crystallinity usually decreases the biodegradation rate as the densely packed crystalline regions prevent the penetration of water and microbial attack. In this study, the inorganic fillers act as nucleating agents and do not show chemical interaction between matrix and filler. It is also true that the biodegradation process is accelerated by the presence of weak interface interactions between polymer and filler.[43] As such, biodegradation is a complex phenomenon depending on various material and environmental properties like molar mass, thickness, filler type and content, porosity, crystallinity, soil type, microorganisms *etc.*, which makes it difficult to predict its biodegradability trend. As a result, each material must be evaluated individually to determine its biodegradable behavior.[2]

4.4. X-ray diffraction

The diffractograms from XRD of talc, $CaCO_3$, and other film samples are shown in Fig. 2(a and b). Talc exhibited its characteristic peaks at $2\theta \approx 9.4$, 19, 28.7, and 36.1°, which correspond to the crystallographic orientations of its (002), (110), (006), and (132) planes, respectively.[44] Similarly, $CaCO_3$ exhibited sharp calcite peaks at 2θ values of 23.2° (012), 29.4° (104), 36.1° (110), 39.6° (113), 43.3° (202), 47.7° (018), and 48.7° (116).[45] The diffraction images of neat TL-PBAT UNST films exhibited a broad amorphous halo, indicating its amorphous nature. The SL and TL composite films containing $CaCO_3$ and talc fillers exhibited characteristic peaks at $2\theta \approx 23.2$, 29.4, 47.7, and 48.7° (for unstretched SL and TL $CaCO_3$ films) and at $2\theta \approx 9.4$, 19, and 28.7° (for unstretched TL talc films), confirming the successful incorporation of the fillers into their respective PBAT matrix.

However, the diffractograms were completely different after the uniaxial stretching of the composite films. For SL-PBAT/$CaCO_3$25% and TL-PBAT/$CaCO_3$25% films at their highest SR value, considerable peak intensity reduction was observed. As such, the peak intensity reduction indicates a change in the crystalline phase, leading to a change in the film's crystal structure. Khan *et al.*[46] in their study on stretched poly(vinylidene fluoride) and barium titanate nanoparticles reported that the shift and reduction of X-ray peaks are associated with changes in the crystal structure. Also, a lack of proper crystalline alignment can result in shorter and broader peaks.[47] A similar trend was observed for TL-PBAT/talc25% films upon stretching.

The $X_{c,xrd}$ values of all the composite films are presented in Fig. 2(c). The $X_{c,xrd}$ of neat TL-PBAT UNST films was 14.9%, which increased significantly to 54.9% for TL-PBAT/talc25% while for SL-PBAT/$CaCO_3$25% and TL-PBAT/$CaCO_3$25% films it was 36.3% and 30.2% respectively. The talc-filled films showed higher $X_{c,xrd}$ than the $CaCO_3$ films, indicating that talc is a better nucleating agent. A similar observation was reported by Leong *et al.*[48] who reported that among talc, $CaCO_3$, and kaolin in polypropylene composites, talc was the most effective nucleating agent. The high aspect ratio of talc creates better contact with the polypropylene matrix, reducing interfacial

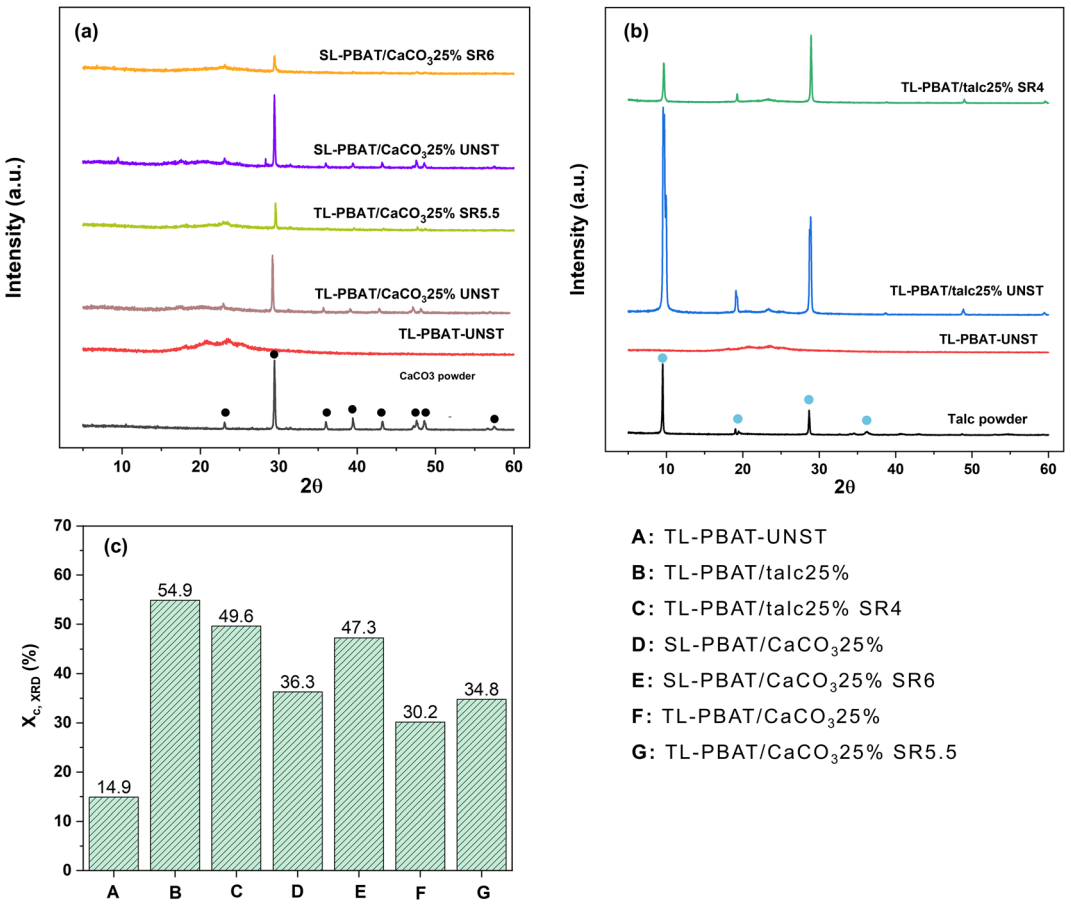

Fig. 2 XRD diffractograms of (a) $CaCO_3$ powder, SL-PBAT/$CaCO_3$25% UNST, TL-PBAT/$CaCO_3$25% UNST and their stretched films; (b) talc powder, TL-PBAT/talc25% UNST and their stretched films; and (c) $X_{c,XRD}$ values of selected films from XRD analysis.

gaps and promoting interfacial nucleation. As observed from the film morphology, talc appeared as well-dispersed, platelet-like particles aligned with the matrix, while $CaCO_3$ showed agglomeration. Additionally, the highly ordered, layered structure of talc and particle orientation increases active nucleation sites within the polymer.[49–51]

This can also be corroborated with the $X_{c,DSC}$, which also shows a higher percentage crystallinity for talc-filled films. Phetwarotai & Aht-Ong (2017)[52] also observed similar results for nucleated PLA films with talc and $CaCO_3$ fillers where the reduced nucleation efficiency observed in the films is attributed to the agglomeration caused by excessive loading of filler particles. They suggested that this occurred because the optimal $CaCO_3$ loading had already been reached prior to further addition. Moreover, the $X_{c,XRD}$ of the film increased after the uniaxial orientation process [Fig. 2(c)]. Both SL and TL PBAT/$CaCO_3$ films showed an increase in $X_{c,XRD}$ at their highest SR. A similar incremental increase in percentage crystallinity after stretching was observed by Jariyasakoolroj *et al.*[53] in biaxially stretched PBS films. However, the TL PBAT/talc films did not show too much variation in $X_{c,XRD}$ before and after stretching. A similar observation was reported by Prieur *et al.*[54] for PBSA and PBSA/silica films. A difference in $X_{c,XRD}$ and $X_{c,DSC}$ values was obtained from DSC and XRD analysis, which could be because of over and underestimation in the DSC baseline used to calculate the enthalpy of fusion, as well as the simultaneous occurrence of thermal phase transitions and melting, which can affect the precision of crystallinity measurements.[30] A key distinction between DSC and XRD measurements is that DSC measure an entire piece of the sample, which is dependent on where it is acquired from (the center or edge), whereas XRD primarily probes the surface of the film as XRD typically penetrates polymer samples to a depth of tens of micrometers and fillers can limit this depth; thus, XRD provides surface crystallinity values, while DSC reflects the overall crystallinity of the entire sample. However, the trends obtained from both studies were similar.

4.5. Dynamic mechanical analysis

Fig. 3 shows the storage modulus and tan δ for the unstretched TL-PBAT/Talc25%, SL-PBAT/$CaCO_3$25%, and TL-PBAT/$CaCO_3$25% films, with their highest SR values. The storage modulus shows how much energy a material can store through its elastic response.[55] From Fig. 3(a), we can observe that the storage modulus of all the samples decreased with an increase in temperature. This phenomenon occurs because increasing

temperature results in higher polymer chain mobility, which results in polymer matrix softening.[56] This marks the onset of transition from a glassy to rubbery state, also known as the T_g.[57] Fig. 3(a) also shows that the storage modulus of the TL talc films was greater than the SL and TL $CaCO_3$ films. This indicates that unstretched talc-filled films had higher stiffness and elastic response than $CaCO_3$ films due to talc's higher aspect ratio than $CaCO_3$ which promotes better dispersion and alignment within the polymer matrix.[51] This enhances stress transfer, enabling the material to resist deformation, leading to a higher storage modulus and elastic performance than $CaCO_3$-filled films. Interestingly, after stretching, the storage modulus of all tested samples decreased drastically. In an unstretched polymer, the chains in the matrix can store energy efficiently during small deformations due to their coiled structure and entanglement. In contrast, highly stretched films exhibit aligned and disentangled chains, and as such, their ability to store energy elastically reduces.

The damping or loss factor ($\tan\delta$) is obtained by dividing the loss modulus by the storage modulus and indicates the energy dissipated by the material during deformation.[55] The peak of the $\tan\delta$ also tells us the T_g of the material. From Fig. 3(b), it was observed that the T_g of neat PBAT and the unstretched talc and $CaCO_3$-filled films exhibited T_g at −20 °C. However, after stretching, the T_g considerably shifted toward higher temperatures. These higher values indicate that stretching restricted the movement of polymer chains. This process reduces the amorphous phase and the available free volume, which limits the movement of the amorphous phase near the strain-included crystallites, which ultimately affects the T_g.[30] This is in accordance with the increase in tensile modulus and reduction in elongation at break observed during mechanical testing.

The $\tan\delta$ graph also provides insights into the filler–matrix interfacial bonding strength: if the talc-based system exhibits a higher storage modulus and a lower loss factor, this can confirm that its interfacial bonding is tighter. As noted previously, the talc-filled TL films exhibited the highest storage modulus and a lower $\tan\delta$ value. This suggests that talc-filled systems had tighter interfacial bonding compared to $CaCO_3$-filled systems. Generally, strong matrix–filler interfacial interactions are represented by a lower $\tan\delta$ peak and T_g shift toward higher temperatures.[58] In contrast, $CaCO_3$-filled TL films show a higher $\tan\delta$ value, suggesting weaker interfacial bonding and more mobile chain segments. The higher chain mobility leads to higher internal friction and is consistent with the lower storage modulus observed, likely due to poorer $CaCO_3$ dispersion.[58]

4.6. Water vapor and oxygen barrier performance

Barriers against moisture and oxygen permeation are key factors in selecting packaging films, and films having lower WVP and OP are preferred in food packaging as they help prevent food spoilage and staleness. Fig. 4 compares the WVP and OP of the developed films before and after stretching. The WVP of the unstretched film of SL-PBAT/$CaCO_3$25% UNST was 612 g mil $(m^2 day)^{-1}$. There was a minor reduction in performance for TL-PBAT/$CaCO_3$25% UNST over the single-layer version as the permeability value increased to 665 g mil $(m^2 day)^{-1}$. However, TL-PBAT/talc25% UNST had a much lower WVP of 308 g mil $(m^2 day)^{-1}$. A similar trend was observed for oxygen permeability for all the films, where unstretched versions of SL-PBAT/$CaCO_3$25% and TL-PBAT/$CaCO_3$25% exhibited OP of 2793 and 2548 cc mil $(m^2 day)^{-1}$, respectively. Here, the TL-PBAT/$CaCO_3$25% had a lower OP compared to its SL counterpart. Also like the WVP trend, TL-PBAT/talc25% UNST had the lowest OP of 1294 cc mil $(m^2 day)^{-1}$. This could be attributed to the platelet structure of the talc filler particles, which increased the tortuosity in the matrix, hindering moisture and oxygen molecules to diffuse easily through the film.[59] Filler morphology plays an important role in moisture and oxygen diffusion through films. Talc, due to its morphological features and high aspect ratio, performs better than $CaCO_3$ against oxygen and moisture diffusion. A similar outcome was observed by Helanto *et al.*[26] for bioplastic film with talc,

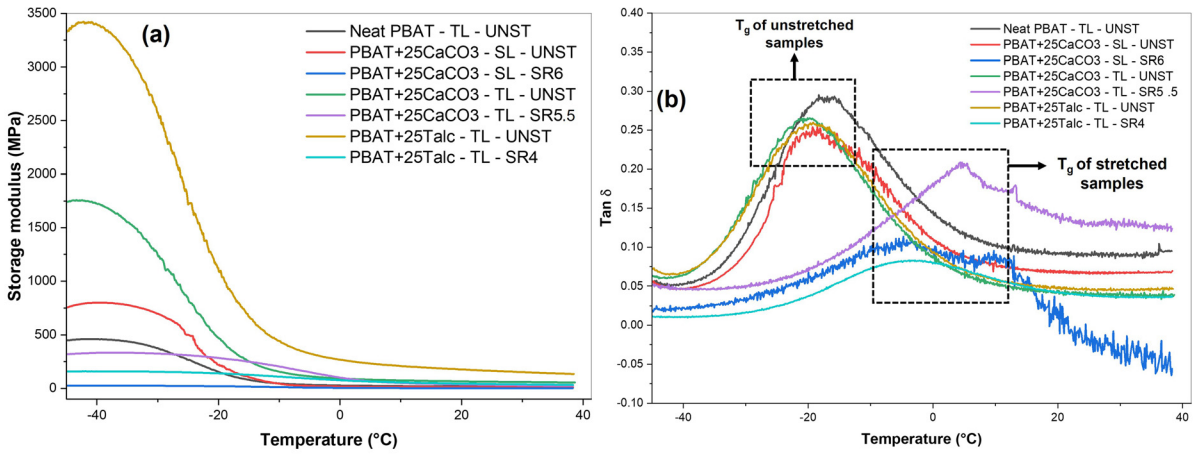

Fig. 3 DMA analysis of unstretched *vs.* highest SR films: (a) storage modulus; (b) $\tan\delta$.

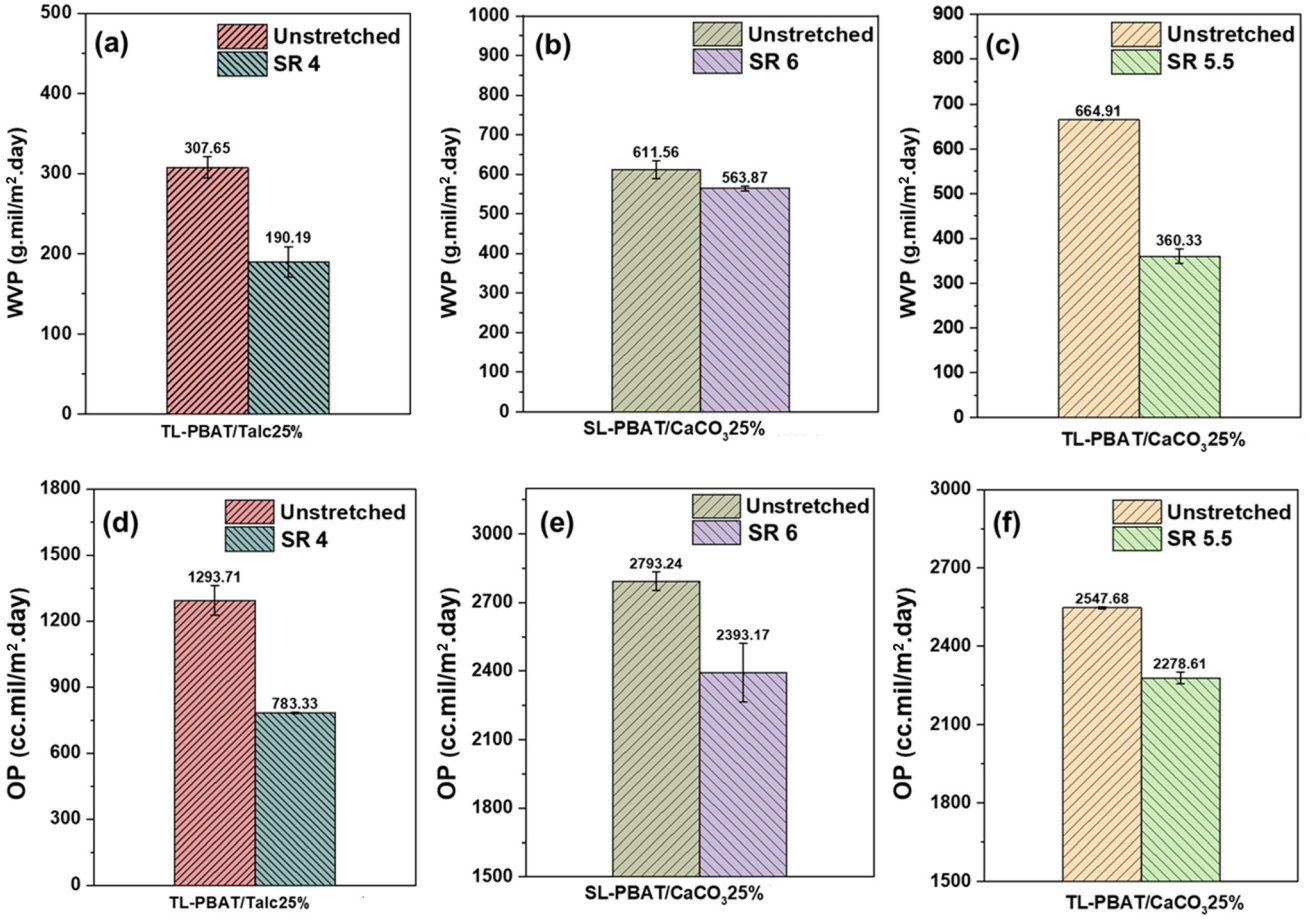

Fig. 4 Water vapor permeability (WVP) of unstretched *vs.* highest SR films: (a) TL-PBAT/talc25%, (b) SL-PBAT/$CaCO_3$25%, and (c) TL-PBAT/$CaCO_3$25%; and oxygen permeability (OP) of unstretched *vs.* highest SR films: (d) TL-PBAT/talc25%, (e) SL-PBAT/$CaCO_3$25%, and (f) TL-PBAT/$CaCO_3$25%.

kaolin, and $CaCO_3$ filler, where talc-filled films showed better barrier performance than $CaCO_3$-filled films.

All stretched films showed a clear drop in WVP and OP at their highest SR. At maximum stretching, the WVP values for SL-PBAT/$CaCO_3$25%, TL-PBAT/$CaCO_3$25%, and TL-PBAT/talc25% were 563.87, 360.33, and 190.19 g mil $(m^2\ day)^{-1}$, respectively. This corresponds to WVP reductions of 8%, 46%, and 38% compared to the unstretched films. Similarly, at the highest SR, the OP values for SL-PBAT/$CaCO_3$25%, TL-PBAT/$CaCO_3$25%, and TL-PBAT/talc25% were 2393.17, 2278.61, and 783.33 cc mil $(m^2\ day)^{-1}$, respectively. These correspond to reductions of 14%, 11%, and 39% compared to their unstretched films. These trends suggest a clear relationship amongst WVP, OP, and SR, which occur because of the orientation of the polymeric chains in the MD, free volume reduction in the amorphous region, and higher crystallinity of the samples that prevents moisture penetration.[19,31]

As per the free volume theory of gas transport, when applied to the two-phase model of semi-crystalline polymers, gases diffuse through the amorphous part of the material while the crystalline regions are deemed as impermeable.[60] These theories explain why the gas permeability of the polymeric materials decreases with an increase in crystallinity and amorphous phase density.[60] Moreover, after stretching, the trilayer films exhibited a better reduction in WVP and OP values. This interesting observation can be justified by the fact that stretching reduces the interlayer distance between the filler and different film layers. As a result, the inter-particle cavities responsible for moisture diffusion are reduced in size, which obstructs moisture molecules from passing through the film.[19]

4.7. Contact angle and surface energy

Contact angle plays a vital role in packaging by indicating surface wettability, which affects both barrier performance against moisture and printability for clear, durable ink adhesion. A high contact angle enhances liquid resistance, while controlled wettability ensures optimal ink spread.[61] The wettability test evaluates how a liquid interacts with a solid surface. When interactions are strong, the contact angle decreases, reducing interfacial tension and allowing the liquid to spread more easily across the material.[62] This property is essential for understanding fluid behavior on different sur-

faces. Hydrophobic materials, which have low water affinity due to their non-polar nature, repel moisture, whereas hydrophilic surfaces attract it. A contact angle below 90° indicates hydrophilicity, while an angle above 90° signifies a hydrophobic surface.[63]

The wettability of the single-layer and tri-layer composite films, along with the neat TL-PBAT UNST sample, was assessed by measuring the contact angles of water and diiodomethane on their surfaces. The results are summarized in Table 4. The images for water and diiodomethane contact angles on the formulations are provided in the SI. The neat TL-PBAT UNST sample showed water and diiodomethane contact angle values of 65.9° and 36.5° (Table 4), respectively. Similar results were reported in the literature.[64,65] The addition of 25 wt% talc to the neat PBAT matrix slightly increased the water contact angle from 65.9° to 70.7°, while no major changes were observed for diiodomethane. A similar result was obtained when 25% silane-treated wollastonite was incorporated into the PBAT matrix for the single-layer film.[7] This increase in water contact angle was attributed to the higher hydrophobicity of the inorganic fillers, which reduced the hydrophilicity of the PBAT polymer matrix. Venkatesan and co-authors[66] developed biocomposite samples using PBAT and kaolin clay at varying concentrations (1–5 wt%). They observed an increase of ~30% in properties when 5 wt% kaolin was incorporated into the PBAT matrix. Uniaxial stretching led to a slight increase in the water contact angle, peaking at approximately 76° at SR 4 for TL-PBAT/talc25% (Table 4). This increase is likely due to the reorientation of talc's platelet structure, which improves molecular alignment and reduces the material's affinity for water, making the surface more hydrophobic. These results are in accordance with those from barrier, SEM, thermal, and XRD analyses.

In contrast to talc, incorporating $CaCO_3$ as an inorganic filler led to a substantial increase in water and diiodomethane contact angles compared to the TL-PBAT UNST sample, with rises of approximately 46% and 99%, respectively, for SL-PBAT/$CaCO_3$25% UNST. Like talc, $CaCO_3$ reduced the PBAT matrix's hydrophilicity due to its inherently hydrophobic nature. The higher contact angles observed for $CaCO_3$ may be attributed to differences in filler shape, orientation, and distribution. Leong *et al.*,[67] investigated polypropylene composites filled with 30% talc or $CaCO_3$ and found that the final properties were largely influenced by the degree of orientation relative to the flow direction. As an anisotropic filler, talc tends to align its plate-like particles parallel to the flow, whereas $CaCO_3$, being isometric, exhibits no preferred orientation, affecting only the overall dispersion within the polymer matrix.

After uniaxial stretching, the water and diiodomethane contact angles of $CaCO_3$-filled PBAT composites decreased from 104° to 74° for TL-PBAT/$CaCO_3$ 25% in the UNST and SR 5.5 samples, respectively, showing the opposite trend observed in talc-filled composites. As previously reported in this work and by Itabana *et al.*,[8] uniaxial stretching promotes the alignment of particles and polymer chains in the MD, particularly for fillers with a platelet structure, such as talc. In contrast, $CaCO_3$, which has a more particulate structure, does not undergo the same reorientation during stretching. As a result, the particles remain in their original positions, creating more cavities within the PBAT matrix and ultimately reducing the material's hydrophobicity. This can also be clearly observed in the SEM images.

Surface energy plays a crucial role in assessing surface wettability and is the reversible work needed to form a unit surface area under constant pressure and temperature. It also provides insight into the material's structural integrity and intermolecular forces.[68] Based on this concept, the TL-PBAT UNST sample exhibited the highest total surface tension, measuring 56 mN m^{-1} and 50 mN m^{-1} using the harmonic and geometric mean methods, respectively, as presented in Table 4. This indicates that TL-PBAT UNST had the highest wettability compared to the other samples. Consistent with the contact angle results, $CaCO_3$ demonstrated a greater ability than talc to increase the contact angle between the polymer and liquid, thereby decreasing surface energy. As the SR increased, the surface energy of the TL-PBAT/talc 25% sample decreased, suggesting lower wettability and a weaker interaction between the surface and liquid. This behavior is because of the alignment of inorganic filler and polymer chains at higher SR levels. On the other hand, the surface energy of $CaCO_3$-filled PBAT samples, both single and tri-layer, increased with the SR.

Table 4 Contact angle and total surface tension (γ_{total}) with polar (γ_p) and dispersive (γ_d) components for SL and TL composite films for the UNST and highest SR samples, along with the neat TL-PBAT UNST sample

	Contact angle (°)		Surface tension (mN m^{-1}@ambient temperature)					
			Harmonic-mean			Geometric-mean		
Formulation	Water	Diiodomethane	γ_p	γ_d	γ_{total}	γ_p	γ_d	γ_{total}
TL-PBAT UNST	65.9 (±1.8)	36.5 (±2.2)	14.5	41.7	56.3	8.9	41.3	50.2
TL-PBAT/talc25% UNST	70.7 (±0.7)	32.5 (±1.5)	12.0	43.4	55.4	6.2	43.1	49.3
TL-PBAT/talc25% SR4	75.7 (±1.5)	32.2 (±0.8)	9.7	43.6	53.3	4.2	43.3	47.5
SL-PBAT/$CaCO_3$25% UNST	96.2 (±0.9)	72.5 (±1.5)	5.2	24.5	29.6	2.3	21.5	23.8
SL-PBAT/$CaCO_3$25% SR6	73.0 (±0.9)	28.9 (±0.3)	10.7	44.8	55.5	4.9	44.7	49.6
TL-PBAT/$CaCO_3$25% UNST	104.3 (±1.2)	68.1 (±2.8)	1.8	26.5	28.4	0.4	23.9	24.4
TL-PBAT/$CaCO_3$25% SR5.5	74.1 (±1.2)	40.0 (±1.2)	10.3	40.2	50.4	5.0	39.6	44.6

As previously mentioned, $CaCO_3$, being a particulate inorganic filler, creates more cavities during stretching, affecting the material properties adversely.

5. Conclusion

This research aimed to investigate the effect of uniaxial stretching on the performance of flexible films with multilayer and single-layer mono-material structures. So, in this study, TL and SL PBAT composite films were prepared with 25 wt% talc or $CaCO_3$ as filler. The composite flexible films were prepared *via* blown film extrusion and underwent MDO. PBAT/$CaCO_3$25% films were prepared in SL and TL configurations, while PBAT/talc25% films were prepared in TL configuration. After stretching, the maximum SR achieved was 4, 5.5, and 6 for TL-PBAT/talc25%, TL-PBAT/$CaCO_3$25%, and SL-PBAT/$CaCO_3$25%, respectively. This variation in the maximum stretching ratio might be due to the higher rigidity and better dispersion of talc fillers, which prevents further stretching beyond SR 4. The mechanical properties of talc-filled films were superior to those of $CaCO_3$-filled films, showcasing talc as a better reinforcing agent than $CaCO_3$. After the uniaxial stretching of the film samples, tensile strength and modulus increased in the MD along with an increase in dart drop impact strength; however, the elongation at break decreased in the MD. Multilayer films showed higher impact resistance compared to single-layer films. The improvement in the performance of the stretched composite films was linked to the increase in crystallinity, molecular chain relaxation, and the orientation of crystalline structures.

Similarly, the OP and WVP barrier properties of the talc films outperformed the $CaCO_3$ films. It is expected that the talc introduces a more tortuous pathway in the polymer matrix compared to $CaCO_3$ due to its platelet-like structure. Moreover, TL-PBAT/$CaCO_3$25% had lower WVP and OP values than SL-PBAT/$CaCO_3$25% samples. Films with the highest SR showed a substantial drop in OP and WVP values. Part of the reasoning for this is due to the polymer matrix becoming more crystalline, hindering the permeation of the molecules through the film. DSC and XRD studies revealed a rise in crystallinity with higher SR, primarily due to strain-induced crystallization, which promoted the formation of additional crystalline structures during stretching. Morphological analysis also confirmed the successful dispersion of inorganic fillers within the polymer matrix, where talc featured a layered structure, whereas $CaCO_3$ tended to form agglomerates. The contact angle study was done to assess the hydrophobicity of the films, and it was found that adding inorganic filler increased the hydrophobicity of the films evidenced by an increase in contact angle. Uniaxial orientation of the films showed a highly aligned matrix in the MD, which can be corroborated by the improvement of the stretched film performance. Overall, uniaxial orientation enhances both mechanical and barrier attributes, making it a method of producing PBAT-filled composites suitable for flexible packaging. This work will help the scientific community with a deeper understanding of the production method of SL and TL film and how the layer configurations affect the performance of stretched and unstretched films for different food and other packaging industries.

Author contributions

Debarshi Nath: methodology, investigation, formal analysis, data curation, writing – original draft. Matias Menossi: methodology, investigation, formal analysis, data curation, writing – original draft. Ehsan Pesaranhajiabbas: methodology, investigation, formal analysis, data curation, writing – original draft. Michael Snowdon: investigation, writing – review & editing and validation. Manjusri Misra: conceptualization, investigation, validation, resources, writing – review & editing, funding acquisition, project administration, supervision. Amar K. Mohanty: conceptualization, investigation, resources, validation, funding acquisition, supervision, writing – review & editing. All authors contributed to the discussion, reviews, and approval of the manuscript for publication.

Conflicts of interest

The authors declare that they have no known competing financial interests or personal relationships that could have appeared to influence the work reported in this paper.

Data availability

The data that support the findings of this study are available within the article and its supplementary information (SI). Supplementary information is available. See DOI: https://doi.org/10.1039/d5lp00306g.

Any additional information required is available from the corresponding author upon reasonable request.

Acknowledgements

The authors would like to acknowledge the financial support of (i) the Ontario Agri-Food Innovation Alliance—Bioeconomy for Industrial Uses Research Program (Project No. 030648, 030671 and 030699); the Ontario Ministry of Agriculture, Food and Agribusiness (OMAFA)-University of Guelph Gryphon's Leading to the Accelerated Adoption of Innovative Research (LAAIR) Program (Project No. 030736); (ii) the Ontario Ministry of Colleges and Universities (MCU), Ontario, Canada Research Fund—Research Excellency ORF-RE11 (Project No. 056106); (iii) the Natural Sciences and Engineering Research Council of Canada (NSERC), the Canada Research Chairs (CRC) Program Project No. 460788; and (iv) NSERC Alliance Grants Program (Project No. 401769) along with the partner industry Competitive Green Technologies, Leamington, Ontario, Canada (Project No. 055427) to carry out this research. The

authors would also like to thank the University of Guelph X-Lab facility for its use.

References

1 Global Plastics Outlook | OECD, https://www.oecd.org/en/publications/2022/06/global-plastics-outlook_f065ef59.html, (accessed 22 February 2025).
2 D. Nath, M. Misra, F. Al-Daoud and A. K. Mohanty, *RSC Sustainability*, 2025, **3**, 1267–1302.
3 D. Briassoulis, P. Tserotas and M. Hiskakis, *Polym. Degrad. Stab.*, 2017, **143**, 214–230.
4 M. Menossi, M. Misra and A. K. Mohanty, *Prog. Polym. Sci.*, 2025, **160**, 101919.
5 A. K. Mohanty, F. Wu, R. Mincheva, M. Hakkarainen, J. M. Raquez, D. F. Mielewski, R. Narayan, A. N. Netravali and M. Misra, *Nat. Rev. Methods Primers*, 2022, **2**, 1–27.
6 K. Das, D. Ray, N. R. Bandyopadhyay, S. Sahoo, A. K. Mohanty and M. Misra, *Composites, Part B*, 2011, **42**, 376–381.
7 M. Menossi, M. Misra and A. K. Mohanty, *Macromol. Mater. Eng.*, 2025, 2400434.
8 B. E. Itabana, A. K. Pal, A. K. Mohanty and M. Misra, *Food Packag. Shelf Life*, 2023, **39**, 101147.
9 R. Venkatesan, K. Alagumalai and S. C. Kim, *Polymers*, 2023, **15**, 1710.
10 Y. Yang, C. Zhang and Y. Weng, *Polym. Test.*, 2021, **102**, 107334.
11 C. Ge and R. Aldi, *J. Plast. Film Sheeting*, 2014, **30**, 77–90.
12 Q. Wang, W. Chen, W. Zhu, D. J. McClements, X. Liu and F. Liu, *npj Sci. Food*, 2022, **6**, 1–16.
13 A. R. Alias, M. K. Wan and N. M. Sarbon, *Food Control*, 2022, **136**, 108875.
14 R. Scaffaro, A. Maio, F. E. Gulino, C. Di Salvo and A. Arcarisi, *Composites, Part A*, 2020, **132**, 105836.
15 F. Palmieri, J. N. A. Tagoe and L. Di Maio, *Materials*, 2024, **17**, 2894.
16 L. Wei, S. Zhan, M. Zhou, X. Xu, F. You and H. Zheng, *Polymers*, 2024, **16**, 2196.
17 D. Guleria, M. Edeleva, S. Vervoort, S. Ge, J. den Doelder and L. Cardon, *J. Plast. Film Sheeting*, 2025, **41**, 35–67.
18 A. Siegmann and Y. Nir, *Polym. Eng. Sci.*, 1987, **27**, 225–231.
19 D. Nath, A. K. Pal, M. Misra and A. K. Mohanty, *Macromol. Mater. Eng.*, 2023, 2300214.
20 H. Y. Nie, M. J. Walzak and N. S. McIntyre, *Polymer*, 2000, **41**, 2213–2218.
21 A. Pietrosanto, A. Apicella, P. Scarfato, L. Incarnato and L. Di Maio, *Polymers*, 2022, **14**, 2759.
22 N. Mallegni, T. V. Phuong, M. B. Coltelli, P. Cinelli and A. Lazzeri, *Materials*, 2018, **11**, 148.
23 F. Chivrac, Z. Kadlecová, E. Pollet and L. Avérous, *J. Polym. Environ.*, 2006, **14**, 393–401.
24 M. Menossi, F. Salcedo, J. Capiel, M. Adler, V. A. Alvarez and L. N. Ludueña, *J. Polym. Res.*, 2022, **29**, 285.
25 P. H. Hermans and A. Weidinger, *Makromol. Chem.*, 1961, **44**, 24–36.
26 K. Helanto, R. Talja and O. J. Rojas, *J. Polym. Eng.*, 2021, **41**, 746–758.
27 K. Helanto, R. Talja and O. J. Rojas, *J. Appl. Polym. Sci.*, 2021, **138**, 51225.
28 G. J. Gill, *Pigm. Pap.*, 2016, 1–8.
29 W. Post, L. J. Kuijpers, M. Zijlstra, M. van der Zee and K. Molenveld, *Polymers*, 2021, **13**, 394.
30 S. Saengbunkoet, N. Kerddonfag, N. Puekpoonpoal, P. Kumsang, R. Yoksan and P. Jariyasakoolroj, *Polymer*, 2022, **249**, 124859.
31 S. H. Tabatabaei and A. Ajji, *J. Appl. Polym. Sci.*, 2012, **124**, 4854–4863.
32 M. Hamdi, M. Puopolo, H. Pham and H. J. Sue, *Tribol. Int.*, 2016, **103**, 412–422.
33 D. Godshall, G. Wilkes, R. K. Krishnaswamy and A. M. Sukhadia, *Polymer*, 2003, **44**, 5397–5406.
34 P. Russo, A. Langella, I. Papa, G. Simeoli and V. Lopresto, *Compos. Struct.*, 2017, **166**, 146–152.
35 M. R. Nobile, A. Crocitti, M. Malinconico, G. Santagata and P. Cerruti, *AIP Conf. Proc.*, 2018, **1981**, 020180.
36 Y. Tao, Z. Mao, Z. Yang and J. Zhang, *J. Vinyl Addit. Technol.*, 2021, **27**, 275–287.
37 H. Moustafa, C. Guizani, C. Dupont, V. Martin, M. Jeguirim and A. Dufresne, *ACS Sustainable Chem. Eng.*, 2017, **5**, 1906–1916.
38 S. Jain, M. M. Reddy, A. K. Mohanty, M. Misra and A. K. Ghosh, *Macromol. Mater. Eng.*, 2010, **295**, 750–762.
39 W. Wu, H.-Y. Mi, C. Huang, H. Zhao, T. Liu, A. Iordanskii, X. Wang, X. Li, L. Cui, Y. Liu and S. Fan, *Polymers*, 2022, **14**, 480.
40 E. Ferrage, F. Martin, A. Boudet, S. Petit, G. Fourty, F. Jouffret, P. Micoud, P. De Parseval, S. Salvi, C. Bourgerette, J. Ferret, Y. Saint-Gerard, S. Buratto and J. P. Fortune, *J. Mater. Sci.*, 2002, **37**, 1561–1573.
41 F. Ma, B. Wang, X. Leng, Y. Wang, Z. Sun, P. Wang, L. Sang and Z. Wei, *Macromol. Mater. Eng.*, 2022, **307**, 2200135.
42 T. Chatterjee, R. Patel, J. Garnett IV, R. Paradkar, S. Ge, L. Liu, K. T. Forziati and N. Shah, *Polymer*, 2014, **55**, 4102–4115.
43 A. Rapacz-Kmita, E. Stodolak-Zych, B. Szaraniec, M. Gajek and P. Dudek, *Mater. Lett.*, 2015, **146**, 73–76.
44 H. Yang, C. Du, Y. Hu, S. Jin, W. Yang, A. Tang and E. G. Avvakumov, *Appl. Clay Sci.*, 2006, **31**, 290–297.
45 Z. Hu, S. Zheng, M. Jia, X. Dong and Z. Sun, *Adv. Powder Technol.*, 2017, **28**, 1372–1381.
46 F. Khan, T. Kowalchik, S. Roundy and R. Warren, *Scr. Mater.*, 2021, **193**, 64–70.
47 M. Fereydoon, S. H. Tabatabaei and A. Ajji, *Macromolecules*, 2014, **47**, 2384–2395.
48 Y. W. Leong, M. B. Abu Bakar, Z. A. M. Ishak, A. Ariffin and B. Pukanszky, *J. Appl. Polym. Sci.*, 2004, **91**, 3315–3326.
49 K. Das, D. Ray, I. Banerjee, N. R. Bandyopadhyay, S. Sengupta, A. K. Mohanty and M. Misra, *J Appl Polym Sci*, 2010, **118**, 143–151.

50 H. Li and M. A. Huneault, *Polymer*, 2007, **48**, 6855–6866.
51 E. Ferrage, F. Martin, A. Boudet, S. Petit, G. Fourty, F. Jouffret, P. Micoud, P. De Parseval, S. Salvi, C. Bourgerette, J. Ferret, Y. Saint-Gerard, S. Buratto and J. P. Fortune, *J. Mater. Sci.*, 2002, **37**, 1561–1573.
52 W. Phetwarotai and D. Aht-Ong, *J. Therm. Anal. Calorim.*, 2017, **127**, 2367–2381.
53 P. Jariyasakoolroj, K. Klairasamee, P. Kumsang, S. Phattarateera and N. Kerddonfag, *J. Polym. Environ.*, 2023, 1–13.
54 M. Prieur, G. Sudre, F. Gouanvé, R. Fulchiron and E. Espuche, *Polymer*, 2024, **304**, 127135.
55 Introduction to Dynamic Mechanical Analysis and its Application to Testing of Polymer Solids - TA Instruments, https://www.tainstruments.com/applications-notes/introduction-to-dynamic-mechanical-analysis-and-its-application-to-testing-of-polymer-solids/, (accessed 15 November 2025).
56 D. Nath, A. Rodriguez-Uribe, T. Wang, M. Misra and A. K. Mohanty, *Int. J. Biol. Macromol.*, 2025, **315**, 144107.
57 S. Paquette, M. Menossi, E. Pesaranhajiabbas, H. Khalil, M. Misra and A. K. Mohanty, *Polym. Compos.*, 2025, 1–18.
58 M. A. Bashir, *Solids*, 2021, **2**, 108–120.
59 Y. Qin, J. Yang, M. Yuan, J. Xue, J. Chao, Y. Wu and M. Yuan, *J. Appl. Polym. Sci.*, 2014, **131**, DOI: 10.1002/APP.40016.
60 Y. J. Lin, P. Dias, H. Y. Chen, A. Hiltner and E. Baer, *Polymer*, 2008, **49**, 2578–2586.
61 S. Krainer and U. Hirn, *Colloids Surf., A*, 2021, **619**, 126503.
62 F. Jahangiri, A. K. Mohanty, A. K. Pal, S. Shankar, A. Rodriguez-Uribe, R. Clemmer, S. Gregori and M. Misra, *Prog. Org. Coat.*, 2024, **189**, 108270.
63 D. Ahmad, I. van den Boogaert, J. Miller, R. Presswell and H. Jouhara, *Energy Sources, Part A: Recovery, Utilization and Environmental Effects*, 2018, **40**, 2686–2725.
64 I. Sifuentes-Nieves, J. F. Hernandez-Gamez, M. Salinas-Hernández, Z. Garcia-Hernandez, A. Herrera-Guerrero, E. Hernandez-Hernandez and P. C. Flores-Silva, *Polym. Compos.*, 2024, **45**, 7564–7573.
65 H. Pan, D. Ju, Y. Zhao, Z. Wang, H. Yang, H. Zhang and L. Dong, *Fibers Polym.*, 2016, **17**, 1540–1549.
66 R. Venkatesan, K. Alagumalai and S. C. Kim, *Polymers*, 2023, **15**, 1710.
67 Y. W. Leong, M. B. Abu Bakar, Z. A. M. Ishak and A. Ariffin, *Compos. Interfaces*, 2006, **13**, 659–684.
68 A. Goswami, S. C. Pillai and G. McGranaghan, *Surfaces and Interfaces*, 2021, **25**, 101143.